The signature of an unbalanced earthquake cycle in Himalayan topography?

Brendan J. Meade*
Department of Earth & Planetary Sciences, Harvard University, 20 Oxford Street, Cambridge, Massachusetts 02138, USA

ABSTRACT

Fifty percent of the relative motion between the Indian and Asian plates is accommodated by active convergence at the Himalayan Range Front (HRF). Earthquake cycle processes on shallowly dipping HRF thrust faults generate large earthquakes ($M_W \geq 7$) and contribute to the growth of HRF topography. Interseismic rock uplift rates reach a maximum north of the active Main Frontal Thrust and have been suggested to significantly influence the collocated convex bulge in HRF topography. Using geodetically constrained models of interseismic rock uplift rates and simple channel erosion rate laws, we show that convex channel profiles are predicted when interseismic deformation outpaces coseismic deformation. Applying this model to the observed elevation profiles of 20 HRF-spanning channels in Nepal yields a minimum mean residual elevation (72 m) if interseismic deformation has outpaced coseismic deformation by a factor of four. The long-term earthquake deficit required for the application of this model is consistent with some estimates of historical moment imbalance but requires temporally variable fault system activity. The spatial correlation between nominally interseismic rock uplift and the HRF topographic bulge may be explained by (1) a noncausal geometric coincidence, (2) geodetic observations of significant deformation not directly related to earthquake cycle processes, or (3) an unbalanced earthquake cycle at the HRF.

INTRODUCTION

The recurrence of large earthquakes along the Himalayan Range Front (HRF) depends on the rate at which elastic strain energy is accumulated (Bilham et al., 1997; Jouanne et al., 2004), transferred, and released (Lavé et al., 2005). Along the Nepal segment of the HRF (Fig. 1A), geodetic measurements of present-day horizontal and vertical interseismic velocities (Fig. 1B) show a pattern of deformation consistent with elastic dislocation models of interseismic strain accumulation north of a shallowly dipping thrust fault with a slip rate of ~20 mm/yr (Avouac, 2003; Bilham et al., 1997; Jouanne et al., 2004) (Fig. 1B). The extent to which interseismic strain accumulation has been balanced by coseismic strain release is fundamental to understanding the nature of the earthquake cycle and seismic hazard. Combined analysis of geodetic slip rate constraints and historical records of earthquake occurrence suggest that over the past 500 yr, coseismic moment release rates have lagged behind geodetically constrained moment accumulation rates by 75%, such that only 25% of the HRF convergence rate has been released through earthquakes (Bilham and Ambraseys, 2005; Bilham et al., 2001). Paleoseismic observations have provided evidence for a great earthquake along the HRF ~900 yr ago, which could have been large enough to balance the millennial moment budget if empirical area-slip scaling laws are not applicable for such large earthquakes (Lavé et al., 2005). To understand whether coseismic and interseismic deformation are balanced over longer time intervals requires a geological record of longer duration than the instrumental or historical periods. Present-day topography is the product of both rock uplift and erosional downcutting and serves as a recorder of the rock uplift signals from both coseismic and interseismic deformation.

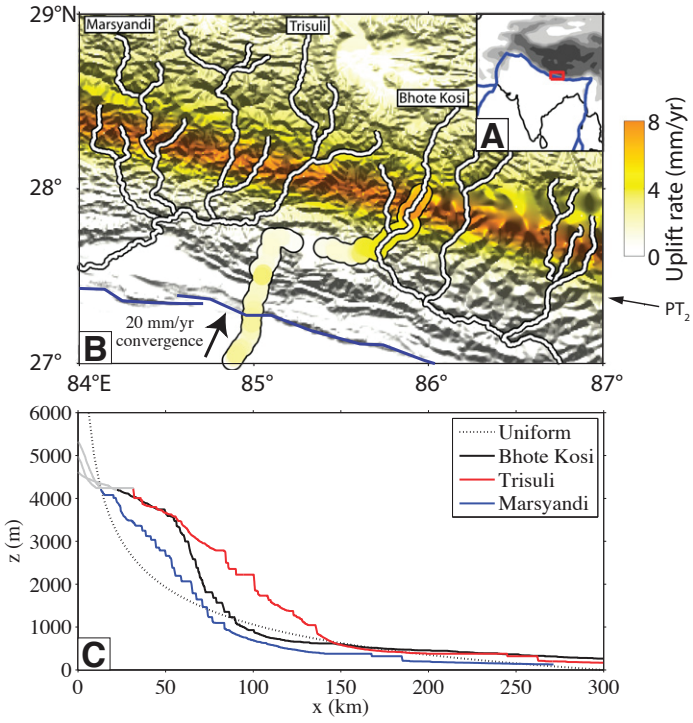

Figure 1. A: Topography at the India-Asia collision zone. Gray shading denotes 1 km elevation contours, plate boundaries are shown as blue lines, and our study area is outlined in red. B: Shaded topography, Main Frontal Thrust fault trace (blue), leveling data (colored circles), modeled interseismic rock uplift rates, and channel locations. Direct observations of present-day interseismic rock uplift rates are only available along the leveling line that runs along the Bhote Kosi (Bilham et al., 1997). We approximate the distribution of interseismic rock uplift along the Nepal segment of the HRF (27°–29° N, 84°–87° E) by fitting fault-perpendicular leveling data using a two-dimensional elastic dislocation model (Bilham et al., 1997) and extrapolating along HRF strike. C: Channel elevation profiles for the Bhote Kosi (black), Trisuli (red), and Marsyandi (blue) rivers derived from 90 m Shuttle Radar Topography Mission (SRTM) topography. The elevation extent of the channel profiles considered here is limited to below 4 km (colored) in order to avoid high elevations that may have been modified by recent glaciations (Gabet et al., 2004). The dotted line shows the classical elevation profile predicted by uniform rock uplift and precipitation rate distributions.

The characteristic form of present-day HRF topography is highlighted in steepest-descent elevation profiles of channels draining southward off of the HRF (Marsyandi, Bhote Kosi, Trisuli) derived from Shuttle Radar Topography Mission (SRTM) data (Farr and Kobrick, 2001). These show that while channel elevations decrease monotonically away from the drainage divide, channel slope and curvature do not (Fig. 1C). This localized channel steepening, or topographic bulge, has been recognized not only in channel profiles (Seeber and Gornitz, 1983) but also as a macroscale physiographic transition with a southern boundary termed PT_2 (Hodges et al., 2001) (Figs. 1B and 2B). Explanations for this aspect of HRF topography have been focused on identifying potential sources

*E-mail: meade@fas.harvard.edu.

of spatially variable rock uplift including midcrustal duplexing (Avouac, 2003), extrusion of lower crustal material (Hodges et al., 2001), and post-Miocene activity on the Main Central Thrust (MCT, near PT_2) (Seeber and Gornitz, 1983; Wobus et al., 2005). Current estimates of the deformation rates associated with out-of-sequence thrusting represent only 0%–10% of the total HRF shortening budget (Wobus et al., 2005), and thermoluminescence dating of fault gouge in the Darjiling sub-Himalaya suggests that out-of-sequence thrusting initiated 20 ± 6 ka (Mukul et al., 2007). Instead, the majority of Pliocene–Holocene surface faulting (21.5 ± 1.5 mm/yr) appears localized 100 km to the south of PT_2 along the Main Frontal Thrust (MFT) (Avouac, 2003; Robert et al., 2009). More resistant crystalline rock units north of PT_2 are also correlated with changes in local channel steepness, but this relationship has been suggested to be, in part, coincidental rather than causative due to the lack of a similar correlation between rock type and topography at the Main Central Thrust (Seeber and Gornitz, 1983).

MODELS OF EARTHQUAKE CYCLE INFLUENCE ON TOPOGRAPHY

Bilham et al. (1997) combined Global Positioning System (GPS) and spirit leveling observations of interseismic surface deformation in Nepal to estimate an MFT slip rate of 20.5 ± 2.0 mm/yr and locking depth of 20 ± 4 km. In addition, Bilham et al. (1997) offered the novel suggestion that "If a fraction of this uplift were nonrecoverable inelastic deformation, permanent uplift of the region would mimic the form of the interseismic deformation field." Here we explore this hypothesis by analyzing HRF channel elevation profiles using quasi-static models of topographic response to both interseismic rock uplift and surface erosion. Interseismic deformation along the HRF is constrained by geodetic observations that show a maximum rock uplift rate north of PT_2 at ~7 mm/yr, approximately three times greater than the far-field rock uplift rate (Bilham et al., 1997) (Figs. 1B and 2C). This effect results from elastic strain accumulation associated with the active MFT, which dips ~4° to the north, and is locked from the surface to the brittle-ductile transition zone, at a depth of 17 km, during the interseismic part of the seismic cycle (Bilham et al., 1997). The surface projection of this rheological transition zone is north of PT_2 and approximately coincident with the topographic bulge (Bilham et al., 1997). Through an idealized, two-stage, earthquake cycle model (Savage, 1983), interseismic rock uplift, U_I, is complemented by coseismic deformation to produce block-like rock uplift of the hanging wall, U_B (Fig. 2C). However, if coseismic moment release does not balance interseismic moment accumulation, then the total amount of rock uplift, U, will deviate from idealized block uplift, $U = \phi U_I + (1 - \phi)U_B$. There are two end-member cases: (1) balanced interseismic and coseismic deformation, $\phi = 0$, and (2) the absence of coseismic activity, $\phi = 1$.

Topography generated by earthquake cycle processes is modified by erosional processes that remove a fraction of the uplifted rock mass. A simple empirically motivated model suggests that erosion rates, E, are controlled by the product of lithologic strength, K, fluvial discharge, Q, and local slope, S, as $E = KQ^mS^n$, where m and n are the discharge and slope exponents, respectively (Whipple and Tucker, 1999). This macroscale parameterization of erosional processes is limited in the sense that it does not directly incorporate the mechanics of sediment transport and bed abrasion (Sklar and Dietrich, 2008) but is rather founded on the assumption that erosion rates are proportional to shear stress, $m/n \approx 0.5$.

Assuming mass flux steady state, where erosion rates balance the vertical, U, and horizontal, V, advection of rock normal to the channel slope, α, and that the average channel slope is the same as the mean topographic slope so that $U \gg V\tan\alpha$ and $E \approx U$, longitudinal elevation profiles may be calculated from the slope distribution if U is known (Whipple and Tucker, 1999). For the simple case with homogeneous lithologic strength, spatially uniform precipitation, and uniform rock uplift rate, $\phi = 0$, predicted channel profiles exhibit a characteristic concave-up shape (Whipple and Tucker, 1999) but do not match the characteristic forms of the large channels along the HRF (Fig. 1C) because this model does not predict a topographic bulge (Fig. 2B). In contrast, the purely interseismic rock uplift rate case, $\phi = 1$, predicts the characteristic features of HRF channels. Model elevation profiles share changes in concavity similar to the Trisuli and Marsyandi Rivers where the excess elevation bulge occurs at 2.5–3.5 km elevation and upstream of the location of maximum interseismic rock uplift (Figs. 1C, 2B, 2C, and 3).

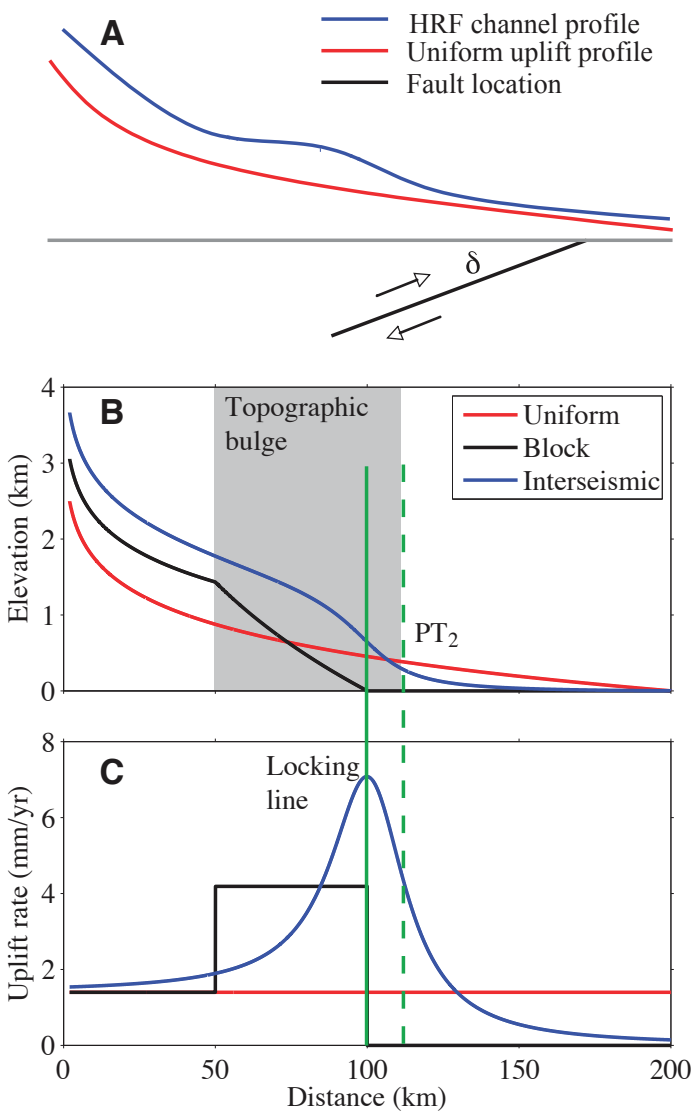

Figure 2. A: Schematic diagram illustrating the geometry and relative locations of the river profiles and the active thrust fault in this model. B: Theoretical longitudinal channel profiles predicted by uniform (red), interseismic (blue), and block (black) rock uplift rates. The elevation profile predicted by the interseismic rock uplift model is defined by the presence of a topographic bulge (gray shaded region) within the hanging wall. C: Uniform (red), interseismic (blue), and block (black) uplift rates. Note that for the block uplift curve, only the hanging-wall component is shown and the footwall is past the right edge of the figure. The maximum interseismic rock uplift rate is located upstream of PT_2 (dashed green line), above the downdip termination of the interseismically locked fault, the locking line (solid green line), and is approximately three times larger than the long-term rock uplift rates in the far field. Note that in both of these cases we are only showing deformation and topography in the hanging wall.

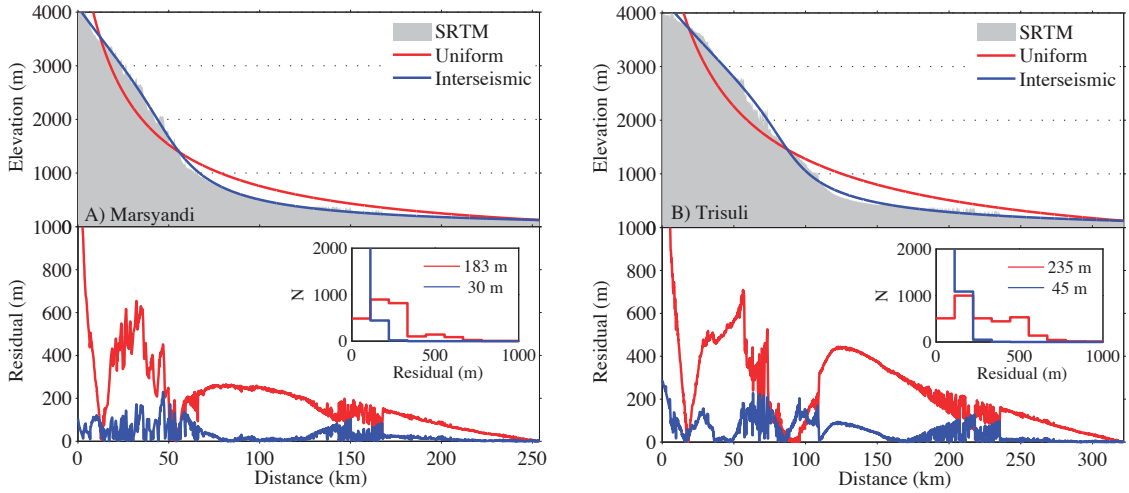

Figure 3. Comparison between observed Shuttle Radar Topography Mission (SRTM) (gray) and modeled elevation profiles. The predictions from the uniform and interseismic rock uplift profiles are shown as red and blue lines respectively in the upper panels. Lower panels show the along-profile magnitude of the residual (SRTM-modeled) elevations. Inset figures show the frequency distributions for the residual elevation magnitudes and mean residual magnitudes for each model. Both the Marsyandi (A) and Trisuli (B) rivers show a distinct bulge in their longitudinal profiles, which is predicted by the excess interseismic uplift model (blue lines).

In general, the entirely unrecovered case, $\phi = 1$, overpredicts the amplitude of the topographic bulge. To determine the fraction of interseismic deformation that has not been balanced by coseismic deformation, we solve for the optimal value of ϕ for 20 channels with accumulated drainage areas >100 km^2 and spaced at ~15 km intervals between 84° and 87° longitude (Fig. 1B; GSA Data Repository[1]). In addition, we use a grid search approach to simultaneously solve for the values of K, m, and n that minimize the minimum norm between observed and modeled channel elevations. We find average values of $\log_{10}K = -1.7 \pm 1.7$, $n = 1.4 \pm 0.2$, and $m = 0.5 \pm 0.2$, giving a concavity index of $m/n = 0.4$, which is within 30% of the theoretical value for a shear stress–dependent incision law $m/n = 0.5$ (Whipple and Tucker, 1999). The covariance between m and K is negative with values along the linear trend from $K = 1$, $m = 0.3$, to $\log_{10}K = -4$, $m = 0.8$ (in $\log_{10}K$ versus m space), predicting channel profiles with the characteristic change in concavity.

Across all channels a minimum mean residual elevation magnitude of 72 m is found at $\phi = 0.8$, while the residual magnitude increases away from this minimum to 128 m and 371 m for $\phi = 1$ and $\phi = 0$, respectively (Fig. 4). For models with a mean residual magnitude <100 m, ϕ varies by less than 10% as a function of erosion law parameters. The model that best predicts the location and magnitude of the HRF topographic bulge is that where only 20% of the accumulated interseismic moment has been released by earthquakes along the MFT.

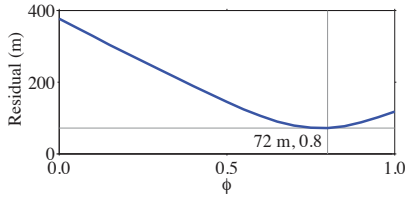

Figure 4. Goodness of fit of the model to topographic data versus fraction of excess interseismic deformation. The average goodness of fit (in meters) averaged over each of the 20 channels is considered (see the Data Repository [see footnote 1] for individual channel profiles). The minimum mean residual of 72 m at $\phi = 0.8$ is associated with a model where only 20% of interseismic deformation has been balanced by earthquake activity.

DISCUSSION

The agreement between model and observations suggests that the erosional response to excess interseismic deformation may have contributed to shaping the topographic bulge at the HRF as suggested by Bilham et al. (1997), consistent with a long-term unbalanced earthquake cycle. Alternative effects may render the possible relationship between topography and interseismic deformation coincidental rather than causal. For example, both the spatial variability in precipitation rates and rock strength may affect channel gradients at the HRF. Precipitation rates perpendicular to HRF strike vary by as much as a factor of five during the annual monsoon (Bookhagen and Burbank, 2006) and have been suggested as a potential mechanism for shaping the topographic bulge and steepening at PT$_2$ (Montgomery and Stolar, 2006). Such precipitation gradients may influence the amplitude of HRF channel slopes (Craddock et al., 2007), but discharge must increase downstream (in the absence of substantial evaporation) and therefore does not produce nonmonotonic trends in channel slope and curvature such as those observed at the convex bulges of HRF channels. Spatial variations in lithologic strength, parameterized as K, have been shown to produce channel profiles with characteristic convex bulges (Stock and Montgomery, 1999). Seeber and Gornitz's (1983) along-strike survey of HRF river profiles noted no strong correlation between rock type and changes in the presence or absence of channel concavity. However, if rock strength is significantly influenced by fracturing associated with earthquake cycle processes or topographic stresses (Molnar, 2004), then rock type alone may be insufficient to quantify the erodibility of HRF material.

In addition to interseismic earthquake cycle activity, spatially variable rock uplift rates may result from out-of-sequence thrusting (Hodges et al., 2001), lower crustal flow (Grujic et al., 1996; Beaumont et al., 2001), or a midcrustal ramp (Avouac, 2003; Robert et al., 2009). The mass flux–conservative Robert et al. (2009) model predicts up to 2.2 mm/yr of vertical uplift above a midcrustal ramp, approaching 30% of the geodetically measured vertical rock uplift rate. Because each of these processes predict rock uplift near PT$_2$, it may be difficult to distinguish between models of interseismic rock uplift rate. If any of these mechanisms actively contribute to HRF growth at rates as little as 20% of the Holocene MFT shortening rate, their activity may be geodetically observable and serve as primary observables of permanent mountain-building processes. However, this would also imply that decadal geodetic velocities are not exclusively produced by interseismic strain accumulation associated with the locked MFT. This assumption is central to the interpretation that geodetic slip

[1]GSA Data Repository item 2010275, observed and modeled river profiles, is available online at www.geosociety.org/pubs/ft2010.htm, or on request from editing@geosociety.org or Documents Secretary, GSA, P.O. Box 9140, Boulder, CO 80301, USA.

rate estimates (Bilham et al., 1997; Jouanne et al., 2004) appear consistent with those averaged over the Holocene (Lavé and Avouac, 2000).

The unrecovered interseismic deformation model links HRF topography to MFT earthquake cycle processes, consistent with Bilham et al.'s (1997) suggestion that interseismic deformation may contribute to the shape of the HRF. The required earthquake cycle imbalance is also consistent with short-term moment balance estimates derived from historical and paleoseismic constraints. Over the past 500 yr, coseismic moment release rates appear to lag behind geodetically constrained accumulation rates by 75%, such that only 25% of the HRF convergence rate has been released through earthquakes (Bilham and Ambraseys, 2005; Bilham et al., 2001). Though the duration of the historical earthquake catalog is ~1/1000 of characteristic topographic response timescales (Whipple and Tucker, 1999), the historical moment deficit appears comparable in magnitude to the topographically constrained estimate, ~20%. However, if sparse measurements of medieval fault rupture are interpreted as evidence for a single great earthquake, larger than any in the historical record, then the HRF moment release rate may be balanced over an ~700 yr interval (Lavé et al., 2005). The unrecovered interseismic deformation model also predicts that the geologic record should reveal evidence for a deficit of coseismic activity, manifest as low paleoseismic slip rate estimates, in contrast to the similarity of Holocene MFT rates (Lavé and Avouac, 2000) and those derived from models of geodetic data (Bilham et al., 1997; Jouanne et al., 2004). Quaternary slip rates would provide additional observations to assess the temporal stability of MFT moment release rates and constrain the extent to which an unbalanced earthquake cycle process may have contributed to the macroscopic form of HRF topography.

ACKNOWLEDGMENTS

Mikael Attal, Jean-Philippe Avouac, an anonymous reviewer, and editor Patience Cowie provided constructive reviews and comments.

REFERENCES CITED

Avouac, J.P., 2003, Mountain building, erosion, and the seismic cycle in the Nepal Himalaya: Advances in Geophysics, Volume 46: San Diego, Academic Press, p. 1–80.

Beaumont, C., Jamieson, R.A., Nguyen, M.H., and Lee, B., 2001, Himalayan tectonics explained by extrusion of a low-viscosity crustal channel coupled to focused surface denudation: Nature, v. 414, p. 738–742, doi: 10.1038/414738a.

Bilham, R., and Ambraseys, N., 2005, Apparent Himalayan slip deficit from the summation of seismic moments for Himalayan earthquakes, 1500–2000: Current Science, v. 88, p. 1658–1663.

Bilham, R., Larson, K., and Freymueller, J., 1997, GPS measurements of present-day convergence across the Nepal Himalaya: Nature, v. 386, p. 61–64, doi: 10.1038/386061a0.

Bilham, R., Gaur, V.K., and Molnar, P., 2001, Himalayan seismic hazard: Science, v. 293, p. 1442–1444, doi: 10.1126/science.1062584.

Bookhagen, B., and Burbank, D.W., 2006, Topography, relief, and TRMM-derived rainfall variations along the Himalaya: Geophysical Research Letters, v. 33, L08405, doi: 10.1029/2006GL026037.

Craddock, W.H., Burbank, D.W., Bookhagen, B., and Gabet, E.J., 2007, Bedrock channel geometry along an orographic rainfall gradient in the upper Marsyandi River valley in central Nepal: Journal of Geophysical Research (Earth Surface), v. 112, F03007, doi: 10.1029/2006JF000589.

Farr, T., and Kobrick, M., 2001, The Shuttle Radar Topography Mission: Eos (Transactions, American Geophysical Union), v. 82, p. 583–585.

Gabet, E.J., Pratt-Sitaula, B.A., and Burbank, D.W., 2004, Climatic controls on hillslope angle and relief in the Himalayas: Geology, v. 32, p. 629–632, doi: 10.1130/G20641.1.

Grujic, D., Casey, M., Davidson, C., Hollister, L.S., Kündig, R., Pavlis, T., and Schmid, S., 1996, Ductile extrusion of the Higher Himalayan Crystalline in Bhutan: Evidence from quartz microfabrics: Tectonophysics, v. 260, p. 21–43, doi: 10.1016/0040-1951(96)00074-1.

Hodges, K.V., Hurtado, J.M., and Whipple, K.X., 2001, Southward extrusion of Tibetan crust and its effect on Himalayan tectonics: Tectonics, v. 20, p. 799–809, doi: 10.1029/2001TC001281.

Jouanne, F., Mugnier, J.L., Gamond, J.F., Le Fort, P., Pandey, M.R., Bollinger, L., Flouzat, M., and Avouac, J.P., 2004, Current shortening across the Himalayas of Nepal: Geophysical Journal International, v. 157, p. 1–14, doi: 10.1111/j.1365-246X.2004.02180.x.

Lavé, J., and Avouac, J.P., 2000, Active folding of fluvial terraces across the Siwaliks Hills, Himalayas of central Nepal: Journal of Geophysical Research, v. 105, p. 5735–5770, doi: 10.1029/1999JB900292.

Lavé, J., Yule, D., Sapkota, S., Basant, K., Madden, C., Attal, M., and Pandey, R., 2005, Evidence for a great medieval earthquake (~1100 A.D.) in the central Himalayas, Nepal: Science, v. 307, p. 1302–1305, doi: 10.1126/science.1104804.

Molnar, P., 2004, Interactions among topographically induced elastic stress, static fatigue, and valley incision: Journal of Geophysical Research, v. 109, F02010, doi: 10.1029/2003JF000097.

Montgomery, D.R., and Stolar, D.B., 2006, Reconsidering Himalayan river anticlines: Geomorphology, v. 82, p. 4–15, doi: 10.1016/j.geomorph.2005.08.021.

Mukul, M., Jaiswal, M., and Singhvi, A.K., 2007, Timing of recent out-of-sequence active deformation in the frontal Himalayan wedge: Insights from the Darjiling sub-Himalaya, India: Geology, v. 35, p. 999–1002, doi: 10.1130/G23869A.1.

Robert, X., van der Beek, P., Braun, J., Perry, C., Dubille, M., and Mugnier, J.L., 2009, Assessing Quaternary reactivation of the Main Central thrust zone (central Nepal Himalaya): New thermochronologic data and numerical modeling: Geology, v. 37, p. 731–734.

Savage, J.C., 1983, A dislocation model of strain accumulation and release at a subduction zone: Journal of Geophysical Research, v. 88, p. 4984–4996, doi: 10.1029/JB088iB06p04984.

Seeber, L., and Gornitz, V., 1983, River profiles along the Himalayan arc as indicators of active tectonics: Tectonophysics, v. 92, p. 335–367, doi: 10.1016/0040-1951(83)90201-9.

Sklar, L.S., and Dietrich, W.E., 2008, Implications of the saltation-abrasion bedrock incision model for steady-state river longitudinal profile relief and concavity: Earth Surface Processes and Landforms, v. 33, p. 1129–1151, doi: 10.1002/esp.1689.

Stock, J.D., and Montgomery, D.R., 1999, Geologic constraints on bedrock river incision using the stream power law: Journal of Geophysical Research, v. 104, p. 4983–4999, doi: 10.1029/98JB02139.

Whipple, K.X, and Tucker, G.E., 1999, Dynamics of the stream-power river incision model: Implications for height limits of mountain ranges, landscape response timescales, and research needs: Journal of Geophysical Research, v. 104, p. 17,661–17,674, doi: 10.1029/1999JB900120.

Wobus, C., Heimsath, A., Whipple, K., and Hodges, K., 2005, Active out-of-sequence thrust faulting in the central Nepalese Himalaya: Nature, v. 434, p. 1008–1011, doi: 10.1038/nature03499.

Manuscript received 3 June 2010
Revised manuscript received 13 June 2010
Manuscript accepted 15 June 2010

Printed in USA